Journal of Seismology **2:** 1–25, 1998.

Effect of non-uniform station coverage on the inversion for earthquake rupture history for a Haskell-type source model

A. Saraò[1], S. Das[2] & P. Suhadolc[1]
[1] *Dipartimento di Scienze della Terra, Università di Trieste, Via E. Weiss 1, 34127 Trieste, Italy*
[2] *Department of Earth Sciences, University of Oxford, Parks Road, Oxford OX1 3PR, U.K.*

Received 4 December 1996; accepted in revised form 8 January 1998

Abstract

In order to determine how reliably one can invert accelerograms to determine the rupture process details, when the station configuration is less than optimal, we use the vertical component of synthetic accelerograms for a Haskell-type earthquake rupture model, at stations in the vicinity of a dip-slip fault and solve the inverse problem. Of the various station configurations used, one is a uniform distribution and the others are very non-uniform. Faults of two different aspect ratios are considered. We mainly use much larger spatial and temporal cell sizes in the inversion than we use to construct the artificial data. The fault mechanism and the fault area are taken as known in the inversions. To solve the inverse problem, we use the method of linear programming and stabilize the solution by the use of physical constraints. The constraints of positivity of the slip rates on the fault is used in all cases in this study. In some cases, additional physical constraints such as preassigning the final moment, the rupture speed, and so on, are also used. We find that using a cell size almost double the wavelength of interest, we are able to reproduce the solution of the problem, even when we add a small amount of random noise to the artificial data, provided the source medium structure is known. We show that the best station configuration is when the stations are on the hanging wall, due to the fact that they provide the best illumination of the fault surface. This provides an incentive to install permanent ocean bottom strong ground motion stations in subduction zones. We also analyzed the effect of the rupture propagation direction on the results of the inversion showing that even four stations are sufficient to retrieve the rupture process if they are in the forward direction of the rupture propagation; the results for this case are better than when the four stations are placed in the backward direction, even when their positions are such that they illuminate the fault in exactly the same way as the four stations in the forward direction. Thus azimuthal distribution and the resulting illumination of the fault as well as the relation of the position of the stations to the direction of rupture propagation are more important than simply the number of stations. Finally, we find that proper knowledge of source medium structure is essential to recover the source process details reliably and that poor knowledge of crustal structure cannot be compensated by adding stations or by additional constraints.

Introduction

The extraction of information about the details of the complete rupturing process of an earthquake by solving inverse problems depends on the availability of high-quality seismograms. Clearly uniform azimuthal distribution of stations around a rupturing fault appears desirable when solving such problems. Since this is often not possible, a study to determine the limitations due to lack of optimal station coverage is important in order to evaluate the reliability of the inverse problem solutions. Some possible configurations of non-uniform station distribution, necessitated by the tectonic and geographic settings, are shown in Figure 1. In many subduction zones, say the circum-Pacific belt, stations are located only on the hanging wall. We call this configuration C-1 in Figure 1(a). In some cases, the stations may be located on the footwall side, as, for example, on the New Guinea subduction zone. We call this configuration C-2 in Figure 1(b). Due to the fact that an earthquake fault may lie partly on land and partly under water, we may have the configurations C-3 and C-4, shown in Figure 1(c). In the Mediterranean area, situations where the stations happen to

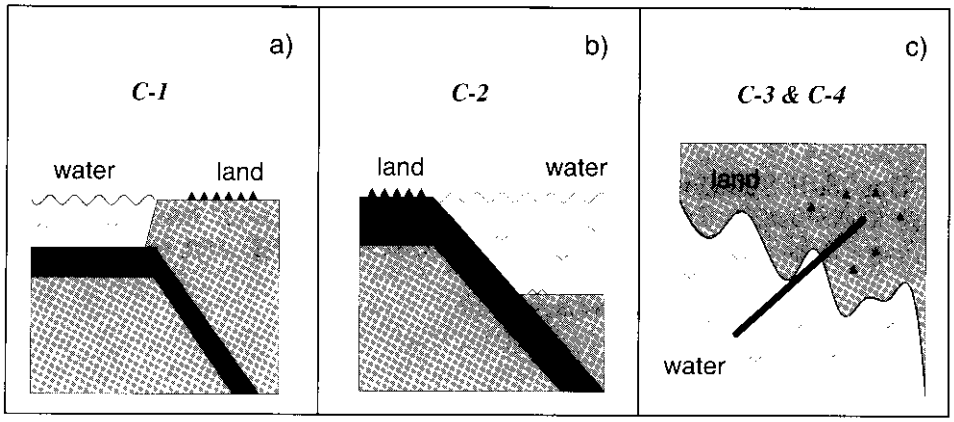

Figure 1. Schematic diagram showing possible non-uniform configurations of seismic stations (solid triangles) relative to an earthquake fault, based on actual situations. (a) and (b) are vertical cross-sections and (c) is a map view; in (c) the thick line is the fault trace.

be at the end of the fault are not uncommon (e.g. the Iberian peninsula, the Messina straits in Italy or on the Yagur fault in Israel). Sometimes this can happen by chance. In Erzincan, Turkey, a single accelerometer was installed in the vicinity of the active fault. When the 1992 earthquake occurred, it was found that the instrument happened to be at one end of the rupture segment (Bernard et al., 1997). There are even geopolitical reasons why stations cannot be placed in the most optimal configuration. The rupture, in such cases, may initiate underwater and propagate towards the stations or initiate under land and propagate away from the stations. Since the effects of the focussing (or de-focussing) of the waves relative to the stations are different in these two cases, we shall consider both these possibilities in this study. We call the case when the rupture propagates towards the station cluster as C-3, and away from the cluster as C-4. The results of our study will help in evaluating the reliability of the moment distribution pattern obtained using very few stations as well as when the azimuthal distribution of available stations is poor. Finally, and not the least important, the results of this study are of practical importance in that they will aid in decisions on the effective (including financial considerations) installation of seismic stations in the field, for example, around recognized active or capable faults.

The problem of non-uniform station coverage has been considered before in moment tensor studies (Stump and Johnson, 1977; Hwang, 1985; Satake, 1985). Olson and Anderson (1988) considered a problem very similar to the one in this paper, for a vertical strike-slip fault. They solved the problem in the frequency domain and used a minimum-norm condition but did not use the physical constraints we use in this paper. Miyatake et al. (1986), Iida et al. (1990), Iida (1993), also carried out a detailed study on the resolving power of strong-motion arrays for source inversion but without any constraints on the solution.

It is well known that such solutions are unstable (Kostrov and Das, 1988; Das and Kostrov, 1990, 1994), and recent work by Das and Suhadolc (1996) and by Das et al. (1996) using vertical component synthetic accelerograms at regional distances has shown that some constraints are essential. In this paper, we shall consider the effect of non-uniform station distribution on the inversion to obtain details of the seismic moment rate history and distribution over the fault for the inversion where additional stabilizing constraints, such as constraining the final moment or disallowing back-slip on the fault, are used. We shall use synthetic accelerograms and stations located at regional distance. One of the reasons we prefer to use accelerograms rather than numerically integrated velocity records, is that it is acceleration that is actually recorded in strong motion investigations. However, the most important reason is to use the data that are most appropriate for retrieving the rupturing process of an earthquake. Madariaga (1977) showed that high-frequency waves are radiated when a rupture front changes speed. Consequently, it is such high-frequencies that must be studied to obtain details of the rupturing process and these are best manifested in measured ground accelerations. The use of the vertical component in the inversion was motivated by several factors. First, at local distances, it is impossible to combine the observed horizontals to get the transverse component of ground motion, as one can do with teleseismic data. So one must use both horizontal

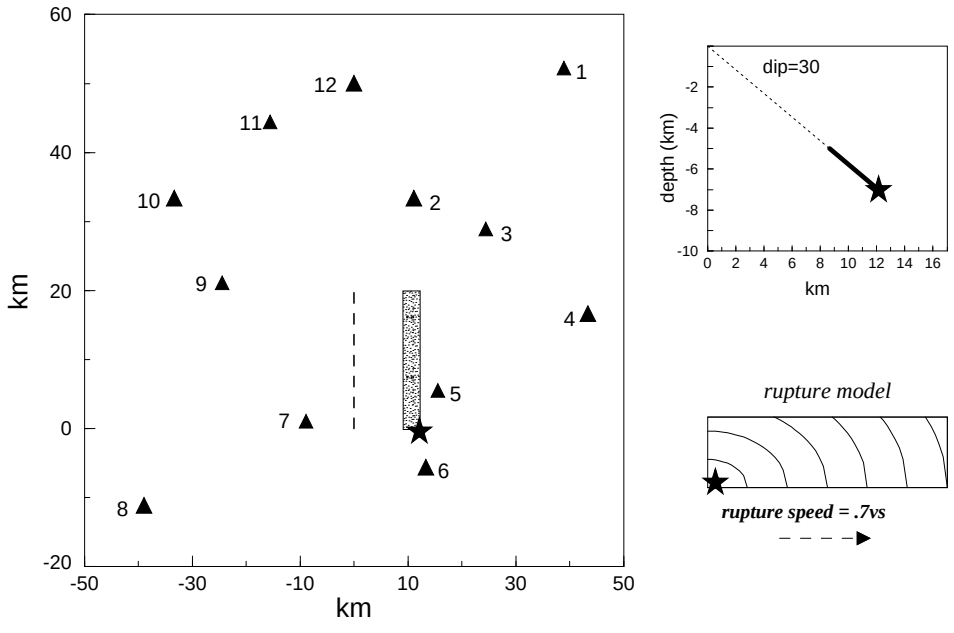

Figure 2. Schematic representation of the dipping fault geometry (cross section on the right) and the 12-station distribution C-0 (plane view on the left) used in this study. The fault dip is taken as 30°. Two different fault aspect ratios (1:5 and 1:2) are used in this study, the fault lengths being taken as 20 km in both sets of cases. The star denotes the hypocenter and the triangles the stations. In the plane view part of the figure, the dashed line is the trace of the buried fault and the stippled fault region is its projection on the horizontal plane. The schematic of the rupture model used in constructing the synthetic accelerograms is also shown.

components in the inversion, thus increasing the number of equations to be solved. This leads to problems related to possible ill-conditioning of the associated matrix, as we shall show in this paper. In addition, use of the vertical components minimizes possible site effects on such records, as it is well known that they are, in general, less sensitive to site effects. Although hard rock site stations are preferable, this is not always possible and stations on 'well-consolidated sediments' or even on unconsolidated sediments might sometimes have to be used out of necessity. Studies using the horizontal components will be the subject of future investigations. Das and Suhadolc (1996) and Das et al. (1996) have shown that with six uniformly distributed stations and a Haskell-type model of the faulting process, some important features remain unresolved even for the problem without any noise in the data. We, therefore, first find the most favourable configuration for which we are able to reliably solve the constrained inverse problem. Once we have done this, we shall perform numerical tests with very non-uniform azimuthal station distributions in order to determine the importance of the station coverage and number of stations necessary to obtain acceptable solutions. We shall consider problems without and with random noise in this study. We shall mostly consider the case when the artificial data is generated using very fine cells and the inversion is performed with much larger cells. Finally, we shall perform the inversion with a different medium than that used in the forward problem. In many of the cases, it may appear that we have deliberately chosen the worst scenario. Since one of our purposes is to find those properties of the faulting process that can be reliably obtained, no matter how unfavorable the scenario, this is desirable. In some real cases the station coverage may be excellent and the knowledge of structural models good, but such cases are globally indeed rare. Most seismic regions of the world are still not well studied and instrumented. In the latter cases the scenario can be even worse than all those discussed in our artificial tests. As a matter of fact, it is very difficult when considering blind test cases as we do here, to

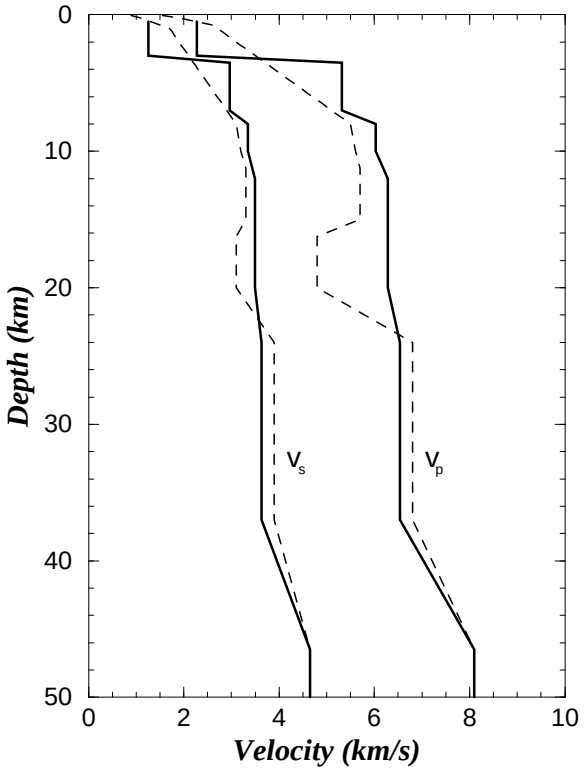

Figure 3. The velocity models used in this study. The solid line shows the structure (M1) used in the forward modeling and in some of the inversions. The dashed line shows an alternative structure (M2) used in some other inversions.

construct the most realistic scenario. Thus, our 'worst case scenarios' may still not be realistic enough, and the real cases may be even worse.

The fault geometry and method of solution

The forward and inverse problems are similar to those described in detail in Das and Suhadolc (1996) and are, therefore, described only briefly here. We construct synthetic vertical accelerograms using the method of multimodal summation for extended sources (Panza and Suhadolc, 1987), for rectangular faults of two different aspect ratios. One fault is taken as 20 km long and 4 km wide, and the other is 20 km $\times$ 10 km. The top of the fault is located at a depth of 5 km and the faulting mechanism is taken as pure thrust, the fault dip being taken as 30°. Since the seismograms for a pure normal fault are the same as for a thrust fault with the sign reversed, our results are also applicable to pure normal faulting with a 30° dip. The schematic fault geometry and an uniform twelve-station distribution is shown in Figure 2 and relevant faulting parameters are listed in Table 1. We shall call the 12-station distribution C-0. The P and S wave velocity models (M1) in the vicinity of the source used in constructing the synthetic data are shown by the solid lines in Figure 3. We shall keep some parameters of the faulting model (namely, the source mechanism, rupture area and the process duration) in the forward and inverse problem the same, since our aim is to study separately the effects of other model parameters, such as different station configurations, different physical constraints, and incorrect Earth structure in the source region, on the solution. The fault is discretized into square cells and the source process duration into discrete time steps. The details of the cell sizes and time steps are listed in Table 1 for all the cases considered in this study. The rupture model is a discrete analog of a Haskell-type model, with rupture propagating at a speed of 70% of the shear wave velocity of the medium. As the rupture passes by, each cell slips only during one time step, in the forward model. An azimuthally uniform idealized distribution of 12 stations (Figure 2) around the fault is used in the first step of this study, while in subsequent cases fewer and very non-uniform station distributions will be considered.

We use the method of linear programming developed for this problem by Das and Kostrov (1990, 1994) for the solution of the set of linear equations $A\vec{x} = \vec{b}$, generated from the elastodynamic representation theorem by the discretization of the problem. A is the matrix of the Green functions, $\vec{b}$ the seismograms and the unknown moment rates are the x's. The physical constraints to be used were enumerated by Das and Suhadolc (1996). We shall require positivity (P) of the slip rate for all cases in this study. The final moment constraint (M), in which the total moment value must equal some pre-assigned value and a rupture speed constraint in which the rupture front is not allowed to propagate faster than some preassigned speed will be considered in some cases. When this limiting rupture speed is taken as the shear wave velocity, we call the constraint R1; when it is 70% of shear wave velocity, we shall call it R1*. A 'weak causality' constraint in which the slip rate is zero in a cell and time step that would produce a signal before the first arrival at any station from the hypocentral cell (R2), may also be used sometimes. A cell may be allowed to slip more than once in the inversion (MTO). The constraints selected in the different cases are also listed in Table 1. We shall define the misfit of the solution synthetics to the

Table 1. Summary of parameters for each station configuration studied

Inversion case	Forward model					Inverse model							Constraints	Noise added	Remarks
	Δx	Δt	nx	nh	nt	Medium	h	Δx	Δt	nx	nh	nt			
	Fault of size 20 km × 4 km														
Case 1:															
Same	2	0.39	10	2	24	*M*1	5	2	0.39	10	2	24	*R*1*	no	All the aspects of
grid													*R*1	no	the solutions
size in													*R*3, MTO	no	reproduced.
forward	1	0.39	20	4	24	*M*1	5	1	0.39	20	4	24	*R*1	no	Instability increases
and													*R*3, MTO	no	as the grid
inverse	0.5	0.39	40	8	24	*M*1	5	0.5	0.39	40	8	24	*R*1*	no	size decreases.
case													*R*3, MTO, M	no	
Case 2:	0.25	0.1	80	16	92	*M*1	5	2	0.39	10	2	24	*R*1*, MTO	no	The fit to
Larger													*R*1*, MTO, M	no	accelerograms
grids in													*R*2, MTO	no	good;
inversion													*R*2, MTO, M	no	the slip rate
													*R*3, MTO	5%	well
													*R*3, MTO, M	5%	reproduced.
Case 3:	0.25	0.1	80	16	92	*M*2	5	2	0.39	10	2	24	*R*3, MTO	5%	Poor
Incorrect													*R*3, MTO, M	5%	solutions.
Earth structure;	Also used only 20s of each accelerogram for C-0 for this case														
larger	0.25	0.1	80	16	92	*M*2	14	2	0.39	10	2	24	*R*3, MTO	5%	Accelerograms
grids in													*R*3, MTO, M	5%	poorly fitted.
inversion															The slip rate best reproduced when all 12 stations used.
	Fault of size 20 km × 10 km														
Case 1	2	0.39	10	5	24	M1	5	2	0.39	10	5	24	*R*3, MTO	no	Same as Case 1 above
Case 2	0.25	0.1	80	40	137	M1	5	2	0.39	10	5	35	*R*3, MTO	no 5%	Same as Case 2 above

Δx is in km; Δt is in seconds; nx = number of cells in which the fault is discretized along the strike direction; nh = number of cells in which the fault is divided along the dip direction; nt = number of steps used to discretize the source time function; h = depth of top of fault in inversion; *R*1: strong causality, rupture front speed constrained to shear wave speed; *R*1*: strong causality, rupture front constrained to move at the 70% of the shear wave speed; *R*2: weak causality; *R*3: without causality.

artificial data, in the ℓ_1-norm sense, as the ratio of the mean absolute error of fit to the mean absolute amplitude of the data (Das and Kostrov, 1990). It should be stated here that comparison of the inversion results with the input is a very strong test of the method and a good comparison between the forward and inverse models is much more revealing than traditional resolution and error matrices. However, in real problems, since there is no other way to estimate the goodness of the result, resolution tests are useful. We do not do such tests here as the simple concept of resolution and error matrices does not hold for the problem where one minimizes the ℓ_1-norm of the residuals. In such cases much more complicated resolution tests, which are beyond the scope of the present paper, would be needed.

More than 110 inversions were performed for this study of which only selected cases will be discussed in detail in the paper. In addition to the ideal distribution of 12 stations (Figure 2), we consider the six non-uniform distributions shown in Figure 4. For each of these station distributions, we consider different combinations of the physical constraints discussed above. For all the above cases, we first perform inversions using the same spatial and temporal cell sizes as used in the construction of the artificial data in order to get

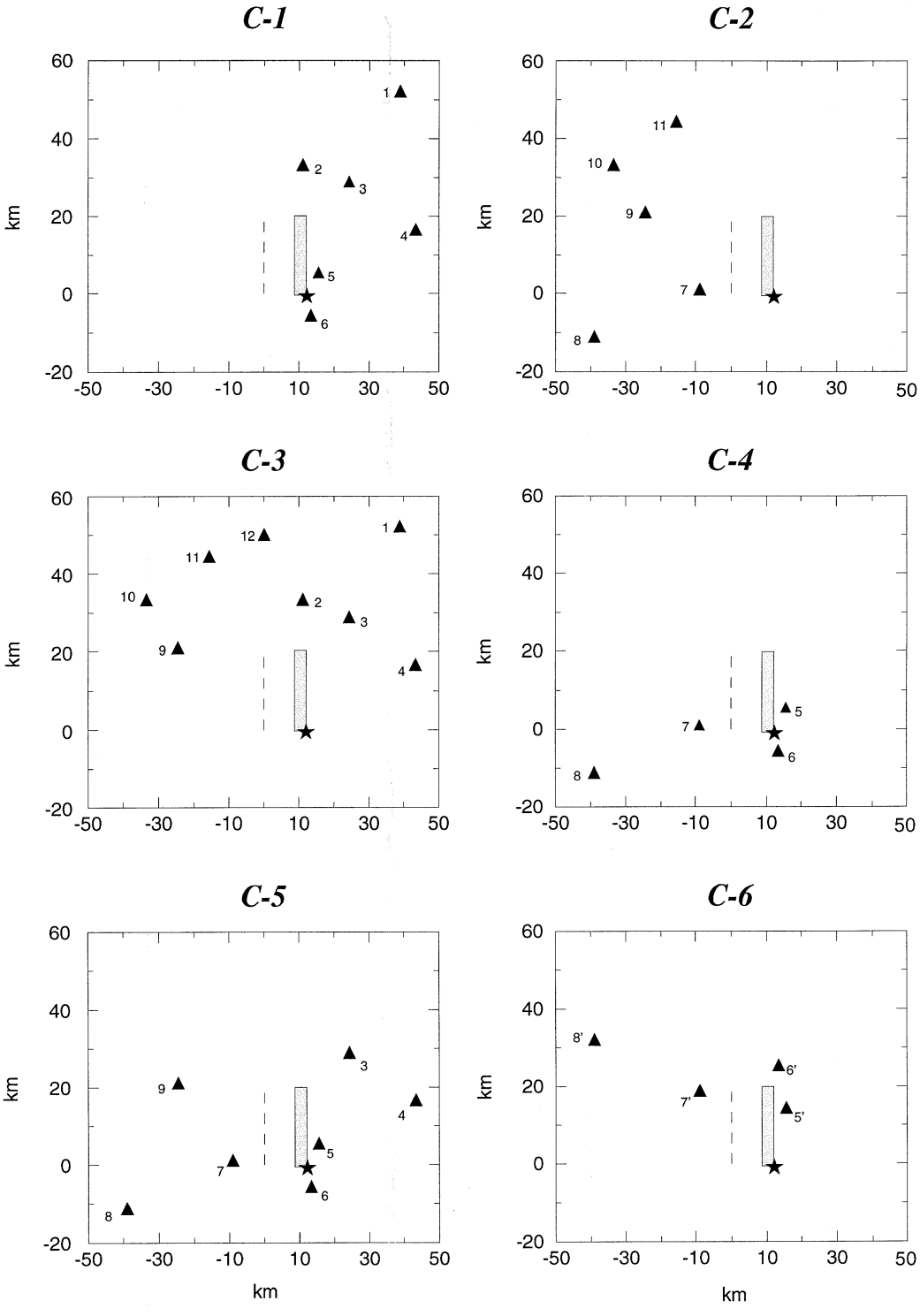

Figure 4. The non-uniform station configurations used in this study chosen to mimic actual possible configurations shown in Figure 1. Two different fault widths are used in this study (the fault lengths are the same in both fault geometries used), but here we plot the fault which is 20 km long and 4 km wide.

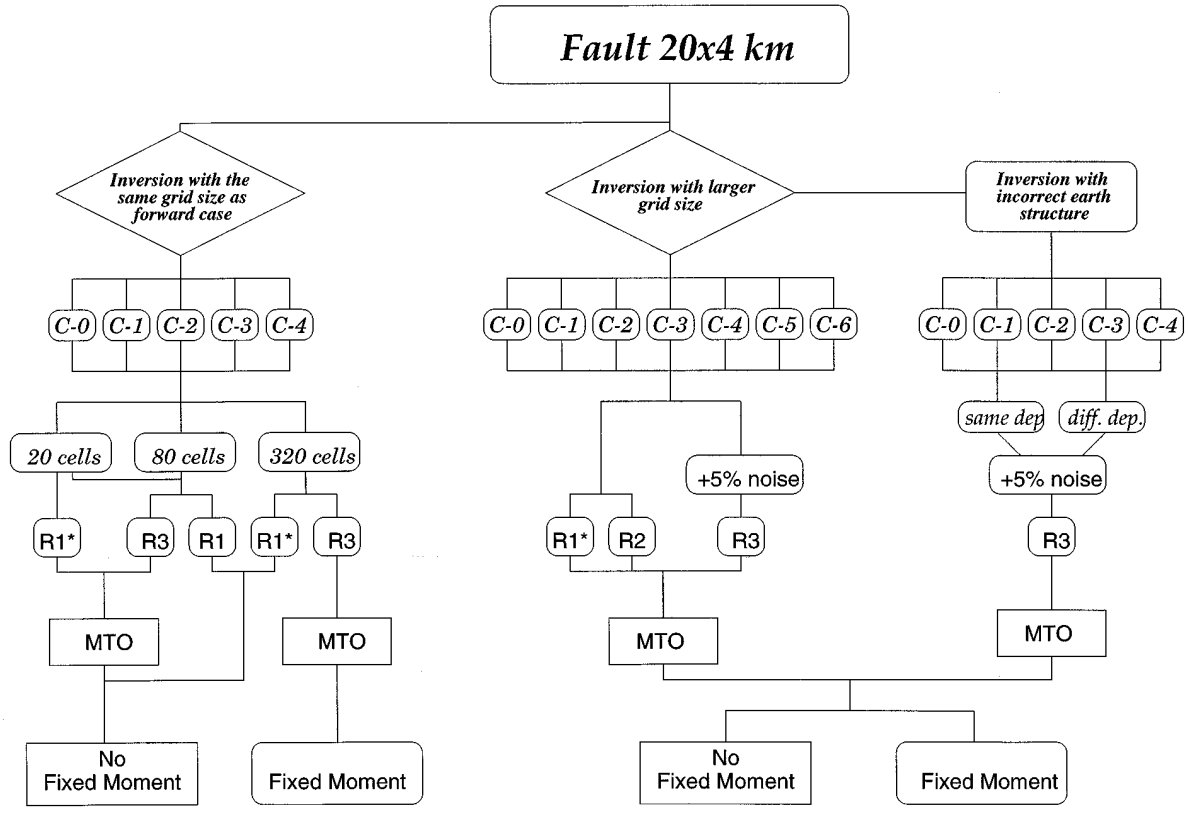

Figure 5a. Chart giving an overview of all the cases considered in this study for the 20 km long and 4 km wide fault. For all the cases, the positivity constraint on the slip rate is used. 'Fixed Moment' denotes the case when the total moment is assigned a priori and 'No Fixed Moment' the reverse. 'R1' denotes strong causality (rupture velocity constrained to be equal to the S wave velocity in the inversion, see Das and Suhadolc, 1996); 'R1*' denotes the case where the rupture velocity is preassigned to be equal to 70% of S wave velocity in the inversion; 'R2' denotes the 'weak causality constraint'; 'R3' is used to identify the case when no causality condition is used. 'MTO' is used to denote the case when grids behind the rupture front are free to slip as often as necessary. In some cases we added 5% of random noise to the artificial data (denoted by '+5% noise'). When using different structures in the forward and inverse problem we perform the inversion for the same fault depth (denoted as 'same dep.') as in the forward problem, and at a different depth (denoted as 'diff. dep.') computed to best agree with the times of first arrival of waves at all the stations.

insight into the inversion. We then carry out inversions using much larger cells in space and time; more than one spatial and temporal cell size will be used in some inversions to investigate its effect on the solution. We shall consider problems with and without random noise added to the data. Finally, we shall perform inversions using 'incorrect' Earth structure. The flow-charts of Figure 5a and Figure 5b give an overall picture of all the cases studied.

Results for the 20 km $\times$ 4 km fault

Case 1: Inversions using the same cell sizes in the inverse and forward cases

The artificial data we use in our tests have been computed using the moment rate distribution, which is obvious ly related to the slip rate by the product of the rigidity modulus and the grid area. In Figure 6, we plot these moment rates, only for the case when the fault is discretized into 20 cells and 24 discrete time steps. This is mainly to facilitate comparisons with inversion results later in the paper. The source medium structure, the fault area, process duration, the depth of the top of the

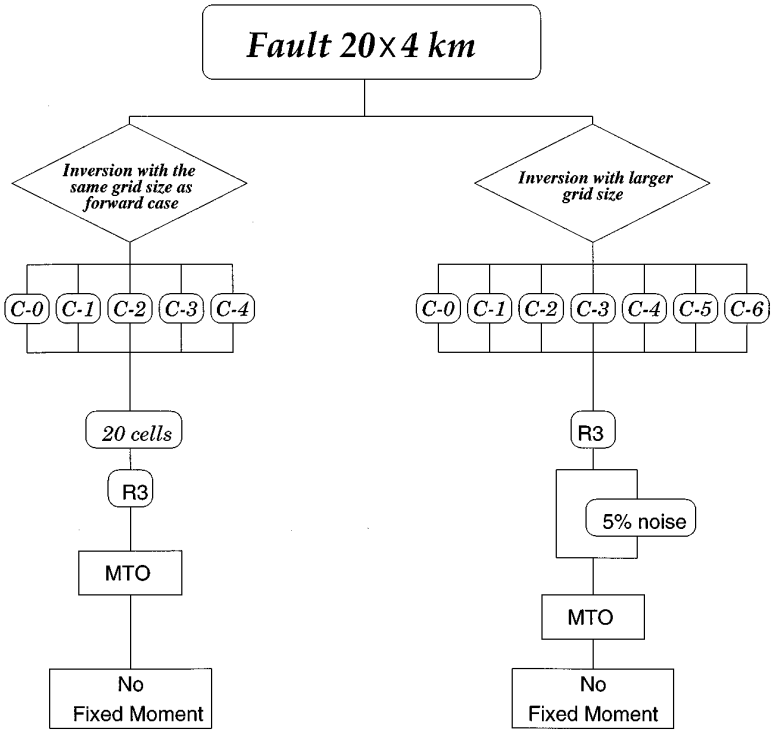

Figure 5b. Same as Figure 5a but for the 20 km $\times$ 10 km fault.

fault (h), and the fault mechanism are the same in the inverse and forward problem, in this case.

To investigate the effect of the spatial cell size on the stability of the inversion, we performed tests using three different cell sizes. We considered square cells of 2 km, 1 km and 0.5 km which correspond to 20, 80 and 320 cells on the fault area, respectively. For each cell size we carried out inversions for the five station distributions (C-0, C-1, C-2, C-3, C-4) using the same cell sizes as in the forward problem and analyzed the effect of the different physical constraints. The source time step size Δt is taken as .39s in this set of cases, for both the forward and inverse problem (Table 1).

Test 1 – This test was carried out primarily as a test of our programs. The rupture velocity is constrained to be the same as in the forward model, each cell is permitted to slip only once as the rupture front passes and the positivity of the slip rate is enforced. All aspects of the solution are correctly reproduced for all the station configurations. Even four stations, grouped together at one end of the fault (C-6), are sufficient to reproduce the rupture process. The solutions are reproduced exactly and the fit to the artificial data is very good so that the differences are not visible on plots, and hence they are not included here.

Test 2 – We perform inversions using the weak causality constraint R2 and do not restrict the cells to slip only once. Again, all aspects of the solutions are well reproduced for all the cell sizes and for all the station distributions.

Test 3 – In this case we do not constrain the rupture front in the inversion, that is, no causality constraint is used. The cells are free to slip more than once and the only constraint used is the positivity of the slip rate. The rupture is free to initiate anywhere within the maximum permitted fault area. This is an interesting case, as, in reality, the rupture front position is unknown and the position of the hypocenter is often quite uncertain. As expected (Das et al. 1996), we found that the stability of the problem decreases as the number of the cells increases. For the model with 20 and 80 cells we were able to reproduce the results without any additional constraints. For the case with 320 cells, the computation time needed was excessive, and we shall see below how to improve this situation in Test 4. The relation between the number of cells and the ℓ_1-norm misfit is

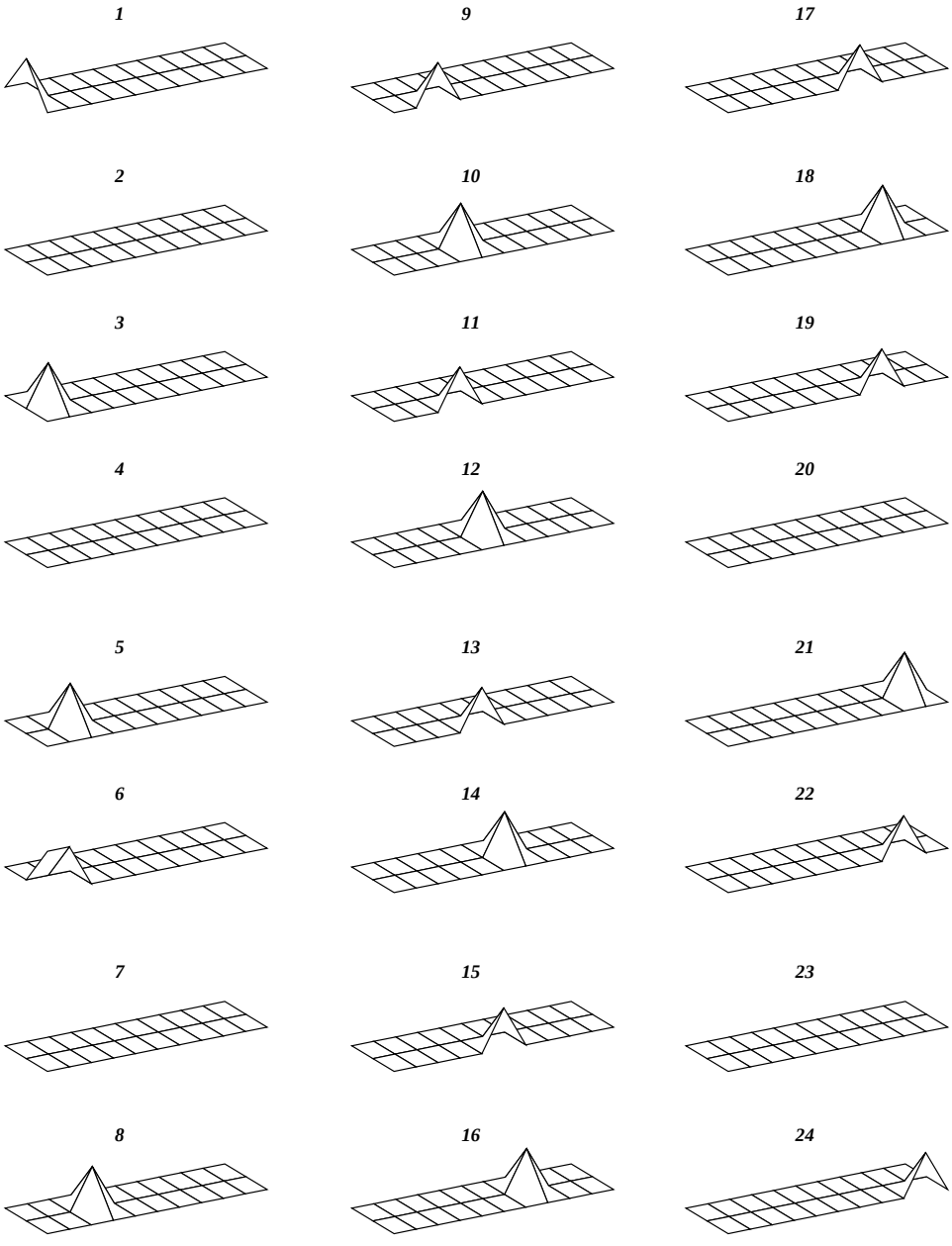

Figure 6. The input moment rate used in Case1 for the fault discretized into 20 spatial cells, is shown at discrete time steps; each step is 0.39s of the source time function. The same plot can be used to compare the inversion results of Case2.

shown in Figure 7. We report for each cell size the misfits for the different configurations. Figure 7 shows that for each cell size the configuration C-1 with the stations on the hanging wall has consistently lower values of the misfit, relative to C-2, with stations on the foot wall.

Test 4 – For the case with 320 cells, we constrained the seismic moment and redid the problem. This reduced the uncertainties in the parameter space and the accelerograms were still fitted well. This demonstrates the necessity of constraints to stabilize the results when using a model with a large number of relatively small cells, as was noted earlier by other authors (Hartzell and Heaton, 1983; Beroza and Spudich, 1988; Das et al., 1996). Clearly, using constraints is one way to reduce the instability of the inverse problem. Next, we

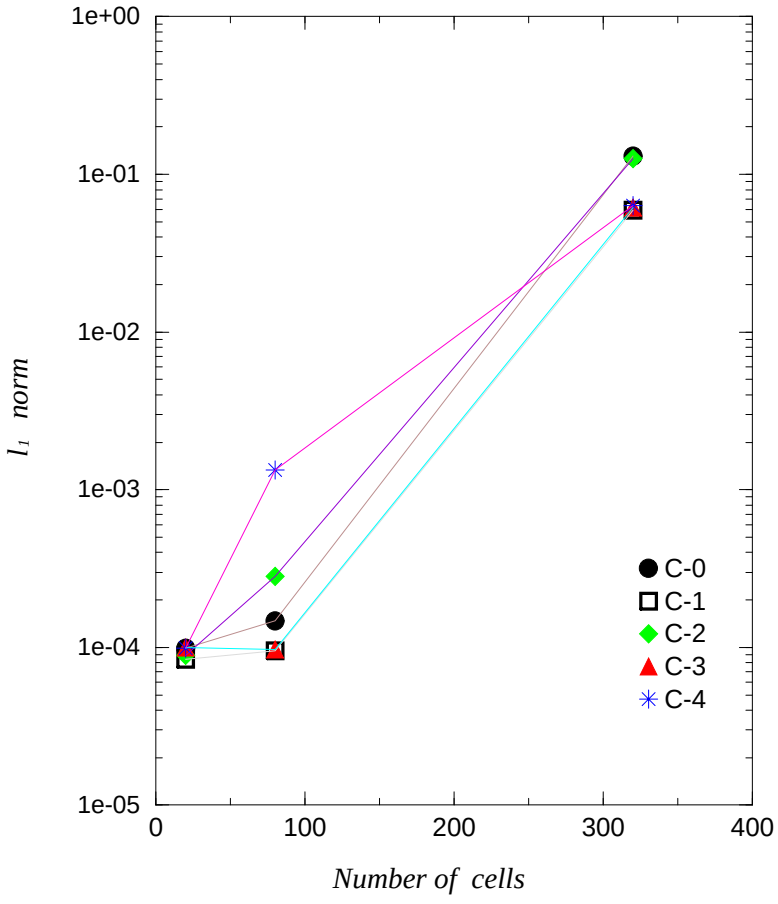

Figure 7. The instability in the solutions when using different cells sizes. The ℓ_1-norm for the five station configurations are plotted against the number of cells.

shall test if it is possible to reduce the size of the matrix and still reproduce the rupture process.

Case 2: Inversion using a larger cell size in space and time in the inverse problem than in the forward problem and with random noise added to the artificial data

We investigate if we can reproduce the total moment rate history and distribution on the fault with a smaller number of cells (that is, larger cells), than that used in the forward problem to generate the synthetic data (Table 1), in order to mimic reality. The accelerograms used as artificial data are computed up to 1 Hz for a cell of 0.250 km. The sampling frequency is 10.24 Hz. This is a reasonably fine discretization for the wavelength of interest in this problem, which is 1.2 km. The cell sizes used for the inversion is 8 times larger in space and 4 times larger in time than the one used in the forward problem. Full details are given in Table 1. We also add some noise to the artificial data in some of the cases (Table 1), in order to mimic not only the 'noise' in the real data mainly due to microtremors not related to the earthquake process, but also to account for the random effect of the 3-D real Earth structure on the signal at any station (the propagation paths from different parts of the fault to the station can be very different). This noise is taken as 5% of the maximum amplitude of the accelerogram at the station, multiplied by a random number. As in Case 1, the source medium structure, the fault area, process duration, the depth of the top of the fault (h), and the fault mechanism are the same in the inverse and forward problem.

Test 5 – We fix the rupture front at its known position and permit the cells to slip only once as the rupture front passes. Even though we reproduce the main features of the solutions, the accelerograms are not perfectly reproduced.

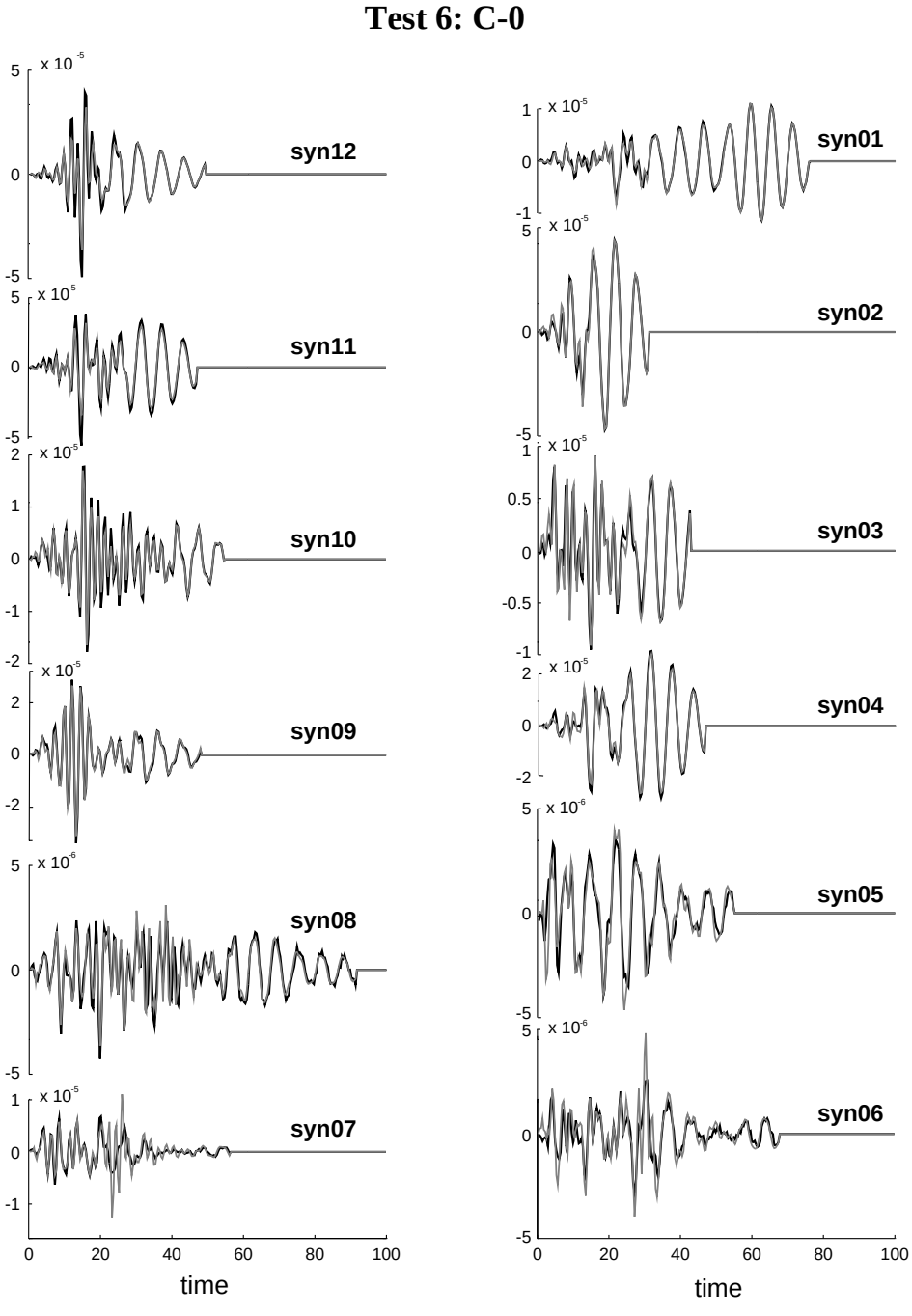

Figure 8. The comparison of the vertical component of the 'artificial data' (solid lines) to the solution accelerograms (dotted lines) for Test 6 of C-0.

Test 6 – We constrain the slip rate to be positive, the cells are allowed to slip as often as necessary and no causality constraint is used on the rupture front. The solution accelerograms obtained after inversion for configuration C-0 are shown in Figure 8. The fit is good and the small differences observed at the stations in the backward direction of the rupture propagation are due to the fact that the amplitudes there are smaller and hence those stations are fit less well than the stations with larger amplitudes. This is also seen by com-

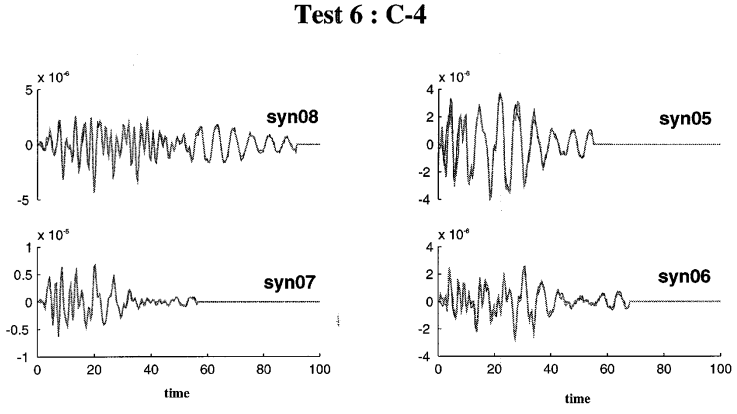

Figure 9. Same as Figure 8 but for Test 6 of C-4.

paring the final relative misfit of the stations among themselves, which shows that the stations in the 'backward' direction with respect to the rupture propagation are less well fitted. In this study we do not normalize the data and we only compare results among configurations which have the same number of stations and same magnitude order of wave amplitudes. By introducing a weight factor before performing any inversion, one could use the mean or the maximum amplitude of the data points at each station as the normalization factor, but we shall not do so in this study.

The waveforms retrieved for configuration C-4, which is one of the cases where the amplitudes of the accelerograms at all the stations used in the inversion are of the same order of magnitude, are shown in Figure 9. The fits of the waveforms improve relative to that for C-0 (Figure 8). The moment rate history and distribution for this test using station distributions C-0, C-1, C-2, C-3 and C-4 are illustrated in Figures 10, 11, 12, 13 and 14, respectively. The best solutions are obtained for C-1. We shall show that this is not only because the stations in C-1 are closer to the fault surface and the physical explanation of this will be given later.

It was not clear if the results obtained for C-4 were relatively poor due to the lower number of stations used in the inversion or due to the particular positions of the stations around the fault. Therefore, we first repeated the inversions for the additional configuration C-5 (Figure 4), using seven stations. C-5 is C-4 but with three additional stations placed in an intermediate position between the forward and backward directions. The fit to the accelerograms obtained for this inversion remains as good as before but the rupture process is now better reproduced. This improvement can be explained by the fact that for C-5, the ray paths from the fault surface to the stations better illuminate the fault area relative to C-4. This is similar to the idea (Menke, 1985) of tomographic imaging of the slip distribution on a fault after an earthquake.

In order to investigate properly the effect of rupture directivity on the inversion, we consider configuration C-6, which is the mirror image configuration of C-4 about the center of the fault, with four stations in the forward rupture direction, so that the fault is illuminated in the same way by C-4 and C-6. We find that the inversion for C-6 is better than C-4 (Figure 15). Thus, the directivity effect plays an important role in how well one is able to retrieve the rupture process details from the inversion. The misfits for the different station distributions are plotted in Figure 16a. Due to the different number of stations used in the different configurations, the misfits are only comparable for configurations C-1 with C-2 and for C-4 with C-6. The lower values of the misfits confirm that the station distributions C-1 and C-6 are better than C-2 and C-4, respectively.

Test 7 – We next constrain the seismic moment to the known value. The moment rate distribution is fairly well reproduced for configurations C-0, C-1, C-2 and C-3 and no slip ahead the rupture front, even though this was permitted in the inversion. We plot only the results for C-2 (Figure 17), and by comparing with Figure 12 for the corresponding case without the moment constraint, we see that solutions did improve. For C-4 (Figure 18), comparing with the Figure 14, we see that the addition of the moment constraint did not improve the solution.

Test 6 : C−0

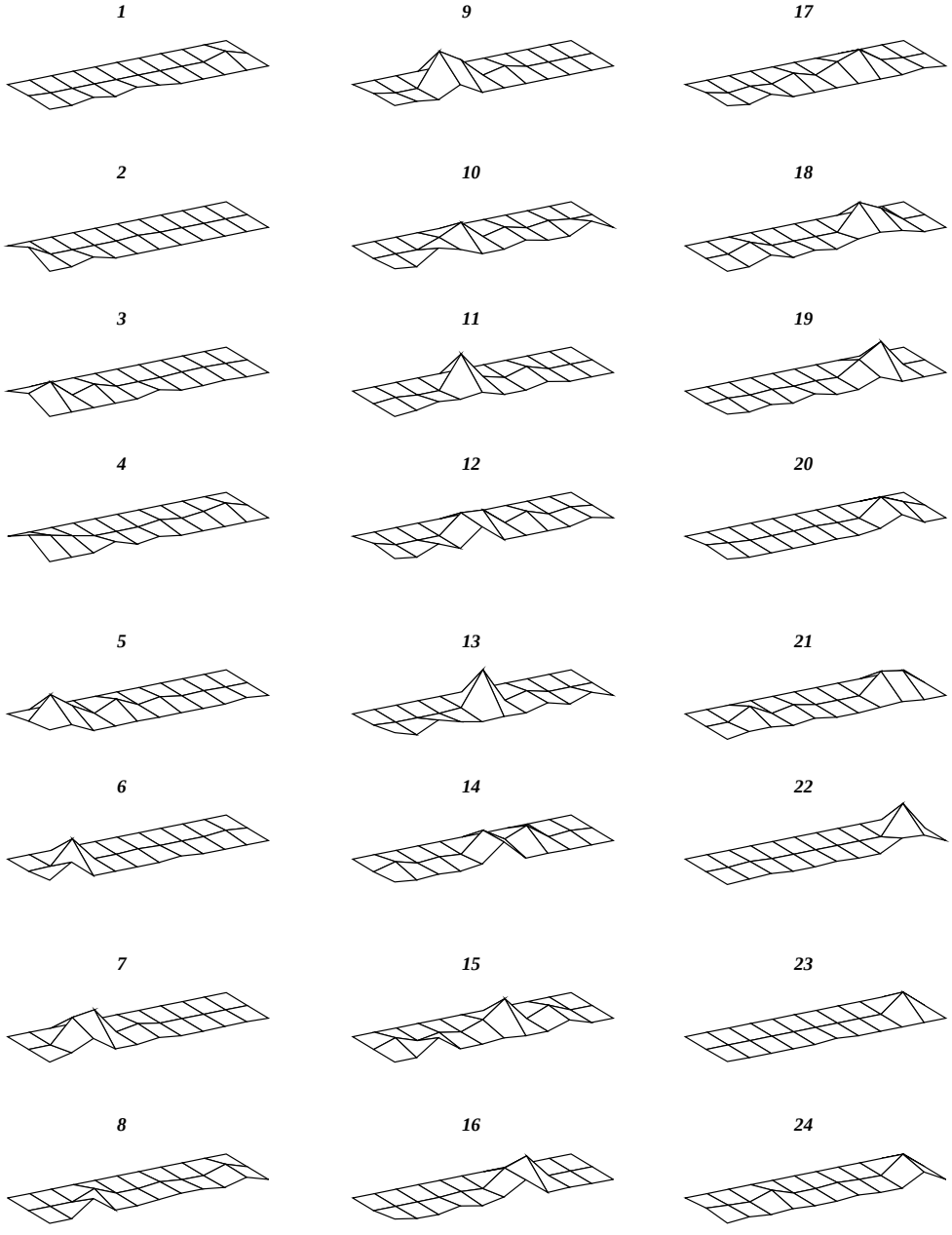

Figure 10. Moment rate map in time obtained by the inversion in Test 6 of C-0.

Test 8 – An unwanted aspect of the solution in Test 6 was the small amount of moment ahead of the rupture front. To eliminate this effect we use the weak causality constraint and grids are permitted to slip more than once. This eliminates the moment ahead of the rupture front but worsens the fit of the accelerograms.

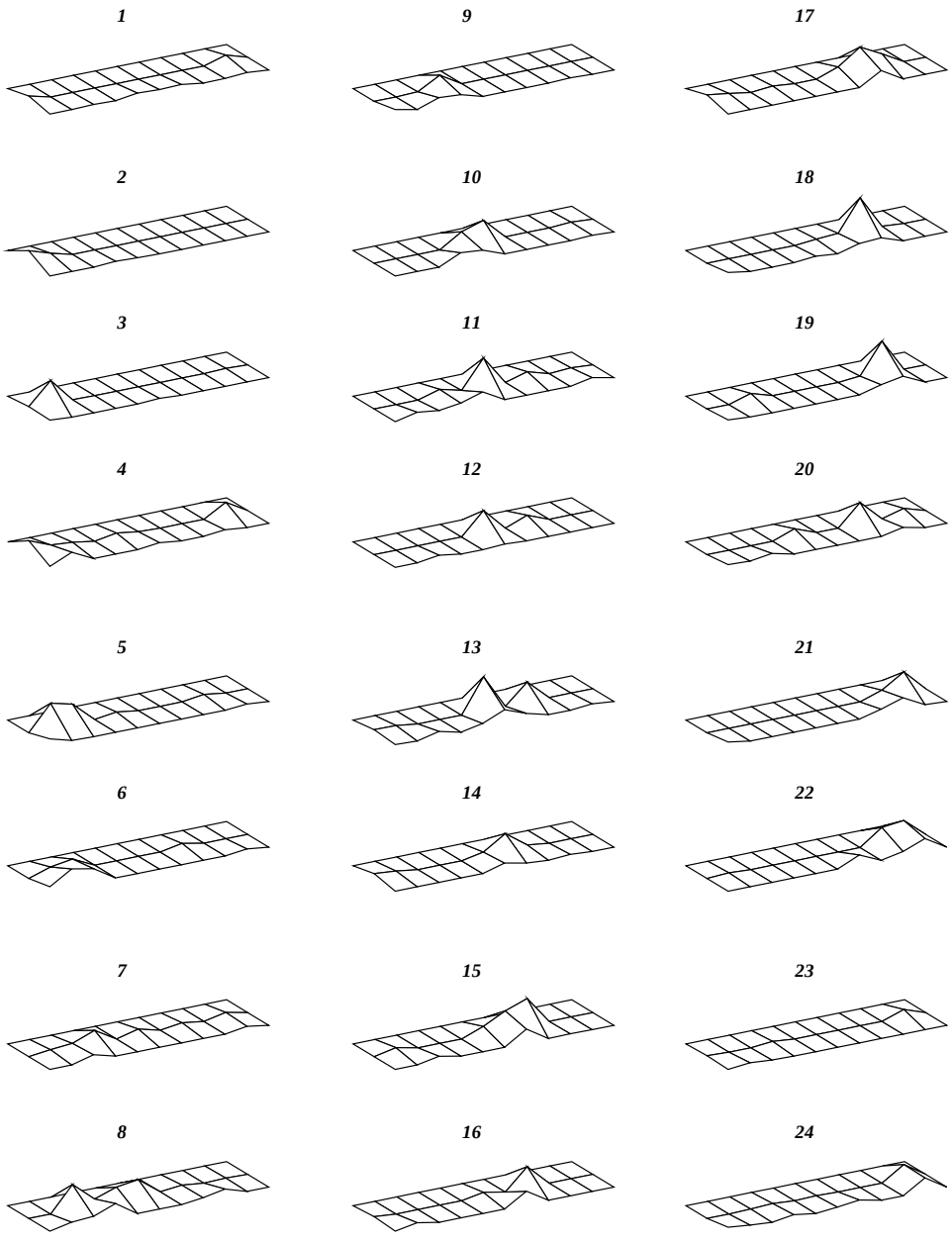

Figure 11. Same as Figure 10 but for Test 6 of C-1.

Case 3: Inversion using a different structure in the forward and in the inverse model

The effect of using an incorrect velocity structural model or an incorrect fault size and depth has been already studied by Das and Suhadolc (1996) and by Das et al. (1996). Using six stations they were unable to reproduce the rupture front correctly. In addition, they

Test 6 : C−2

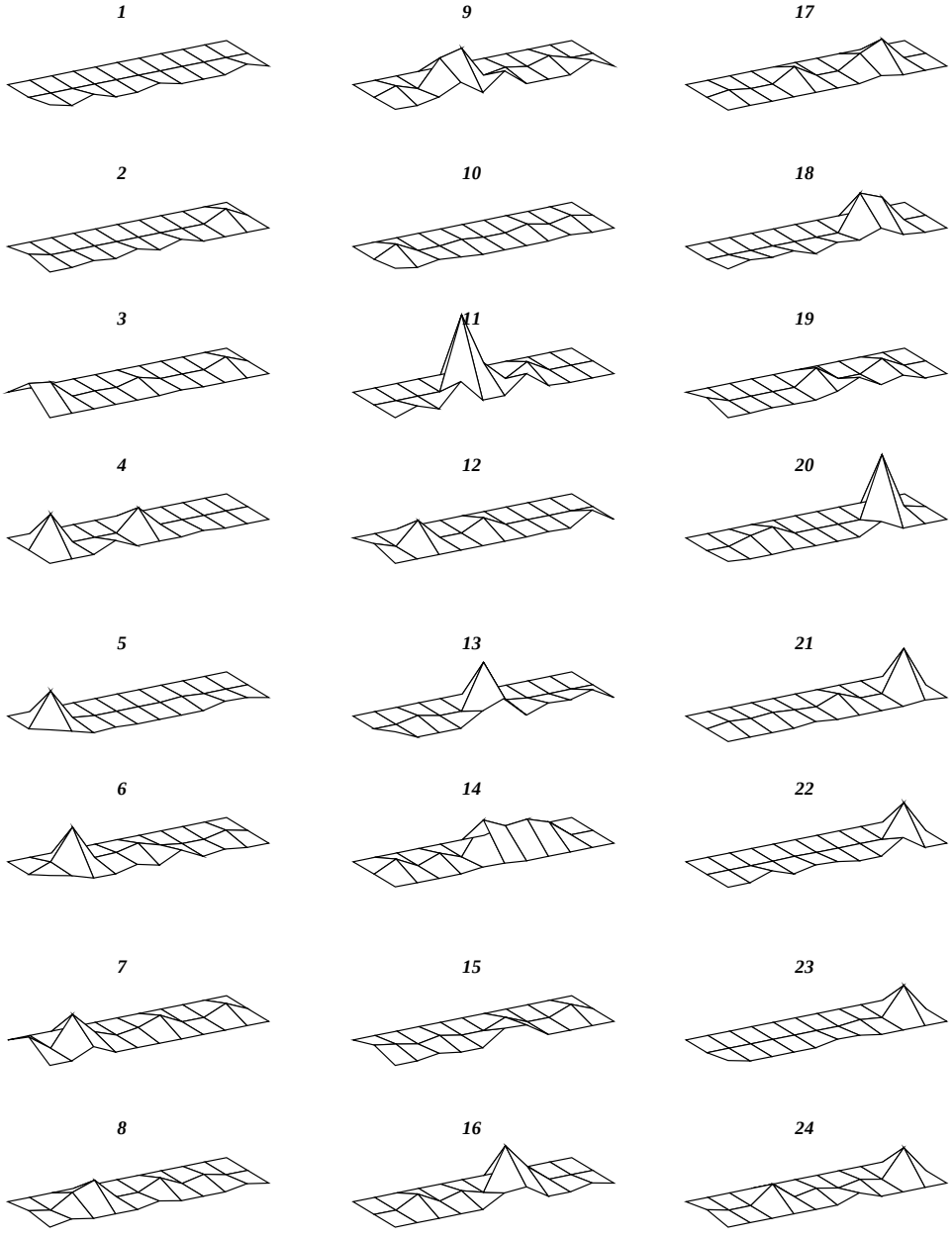

Figure 12. Same as Figure 10 but for Test 6 of C-2.

obtained some systematic moment behind the actual rupture front, which they called ‘ghost front’. Here we study the effect of using an incorrect structure in the inversion when the inversion is performed using larger gridding than the forward problem, and when the artificial data also have some random noise added.

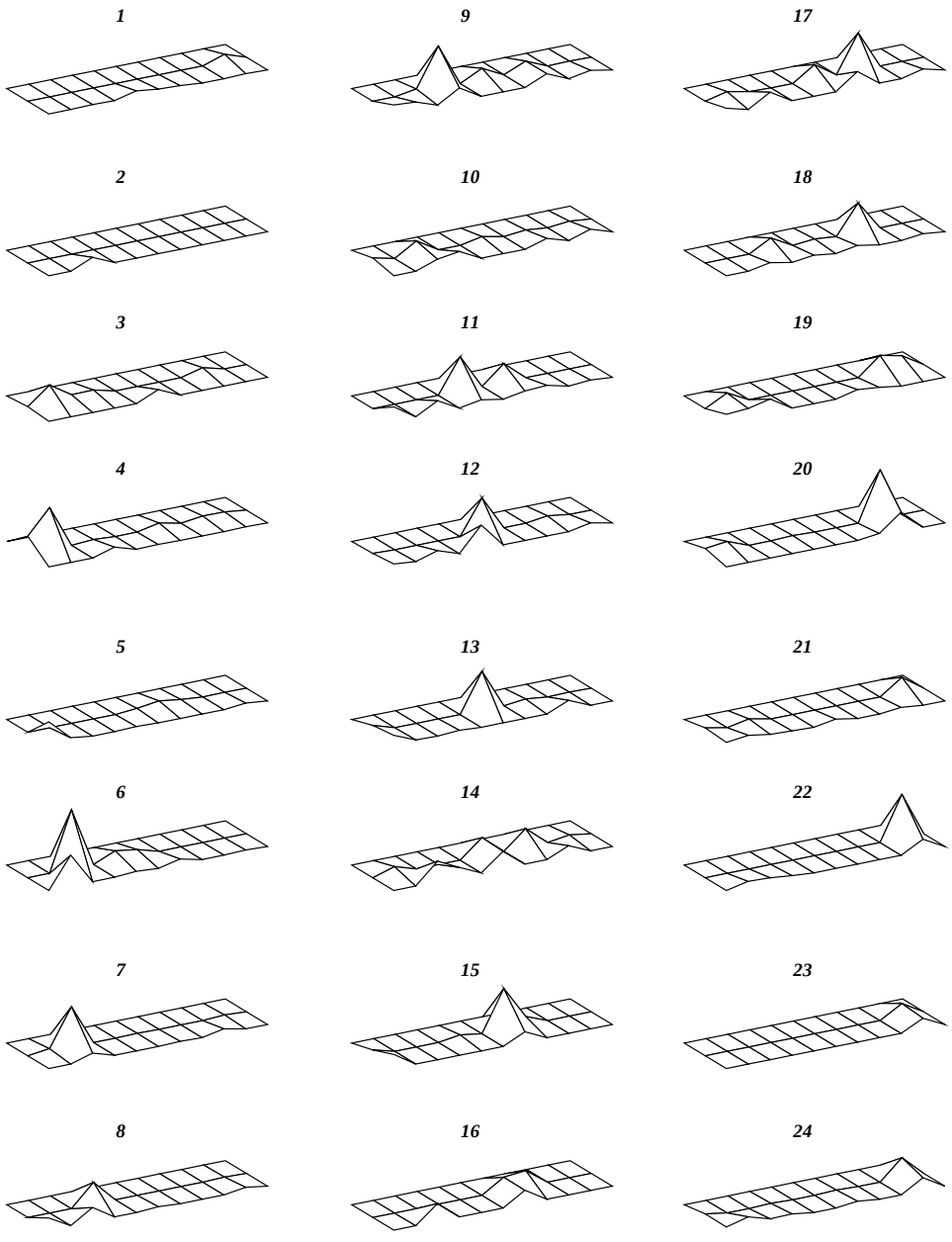

Figure 13. Same as in Figure 10 but for Test 6 of C-3.

The artificial data are computed for a spatial cell size of 0.250 km with a sampling frequency of 10.24 Hz in the medium M1 (solid line in Figure 3). The Green functions used in the inversion are computed for a cell size of 2 km and a temporal step of 0.8s with the structural model M2 (dashed line in Figure 3). The two structural

Test 6 : C−4

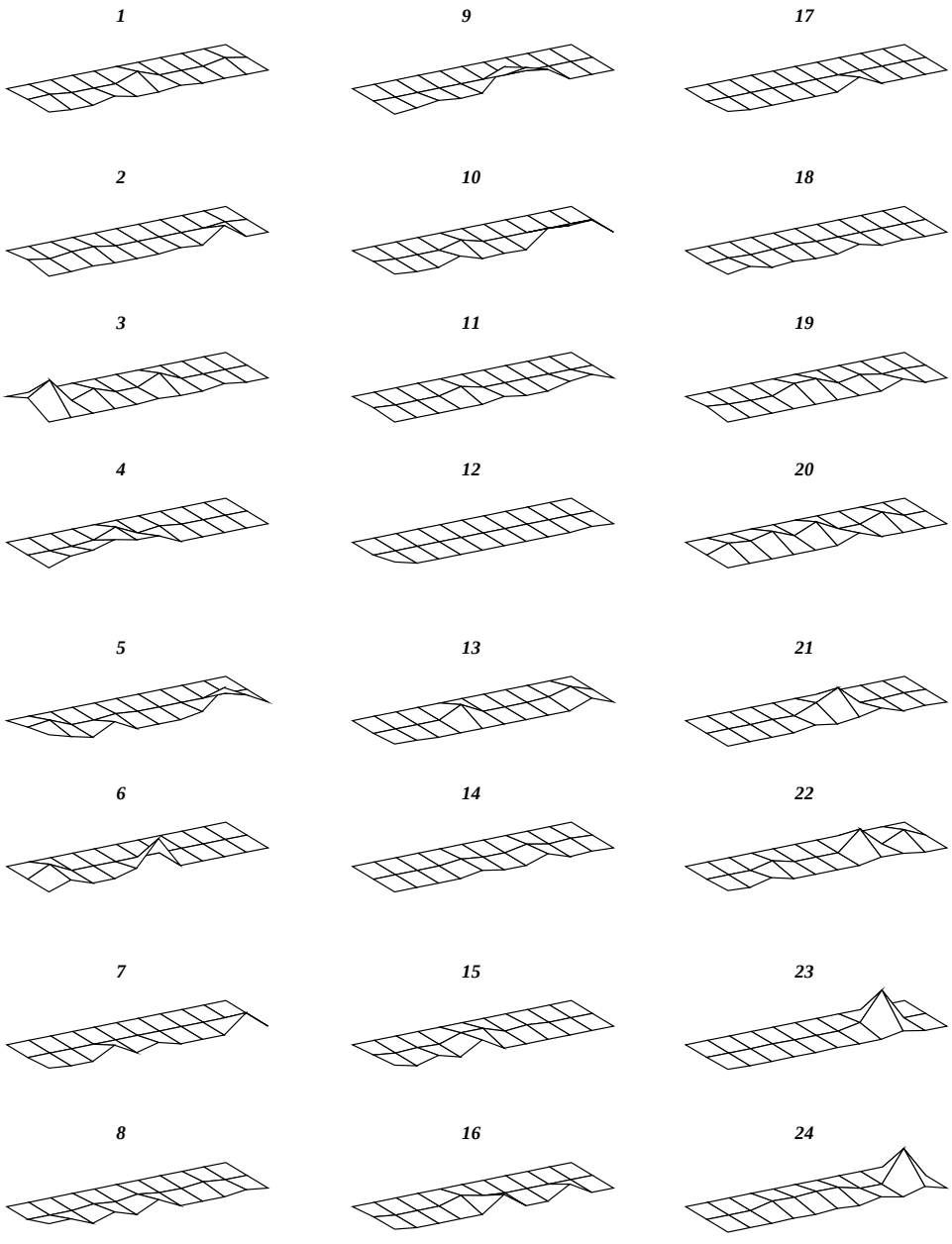

Figure 14. Same as in Figure 10 but for Test 6 of C-4.

models are deliberately chosen to be quite different to analyze a very unfavorable scenario. In most regions of the world, the velocity inaccuracies due to a poor knowledge of the structure are substantially larger than those in the very few well-investigated regions of the

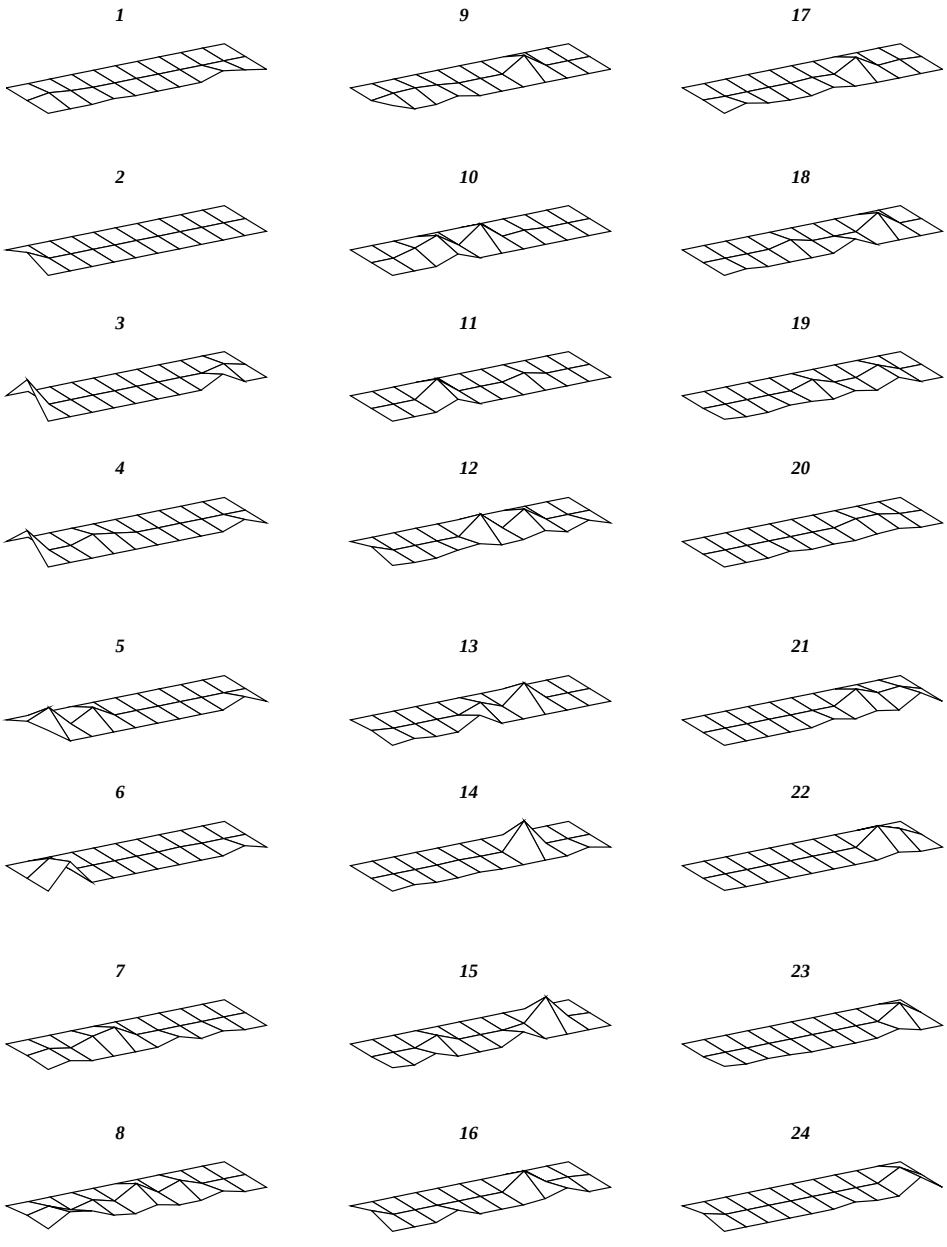

Figure 15. Same as in Figure 10 but for Test 6 of C-6.

world. The fault area and the fault mechanism are the same in the inverse and forward problem.

Test 10 – The fault model of the inversion has the same size, and for this test the top of the fault is placed at the same depth as that in the forward model. We fix the slip rate to be positive and the cells are free to slip as often as necessary. No causality condition is imposed on the rupture front. For all the station distributions we find that the fit of the accelerograms is poor and the rupture process is not well reproduced.

Test 11 – The moment value is fixed in the inversion and we use the same fault model as in Test 10. The fit

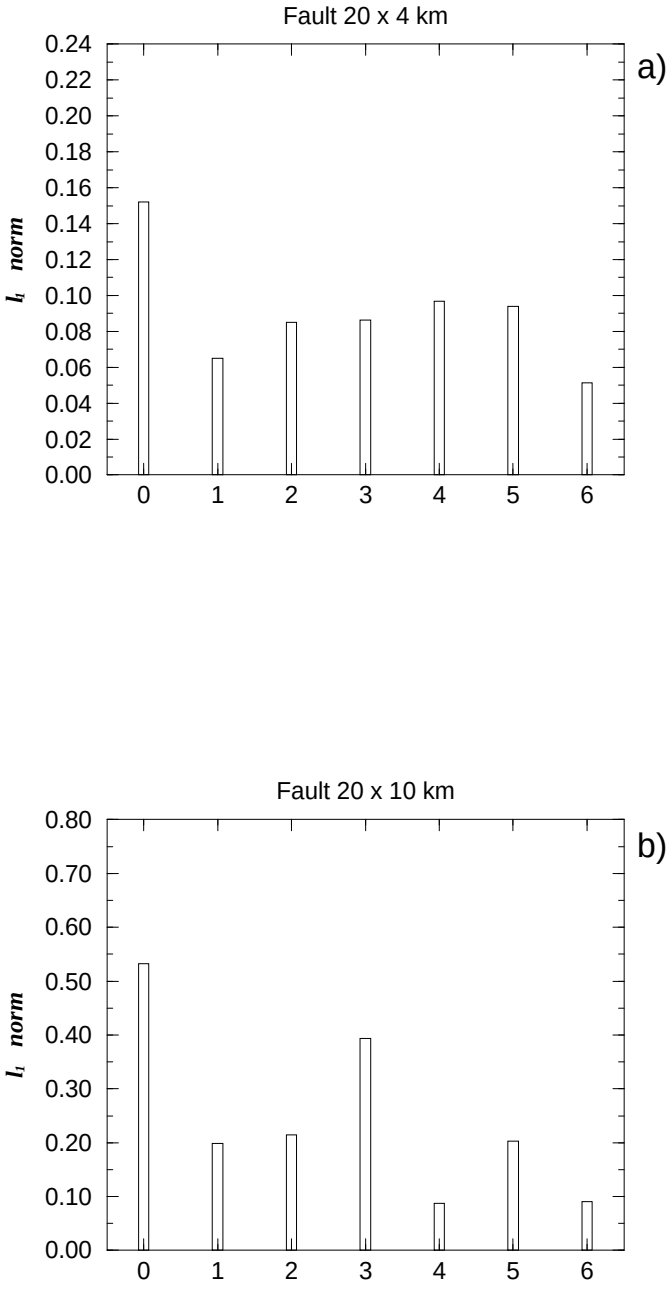

Figure 16. Misfits for different station configurations for (a) the 20 km $\times$ 4 km fault (b) the 20 km $\times$ 10 km fault.

of the accelerograms does not improve and the rupture front is still not well reproduced.

Test 12 – We place the fault with its top at a depth of 14 km. At this depth the first arrival times are compatible with those obtained for the forward case. The solutions are not well reproduced even with additional constraints. The fit of the accelerograms is shown in Figure 19 and the moment rate in Figure 20. We can identify the rupture front and we do not see any other systematic moment rate behind or ahead of the rupture front. However, a few, small scattered areas with non-zero moment rates are seen over the fault surface, including in the acausal regions. Fixing the value of moment does not improve the results. Thus, we are

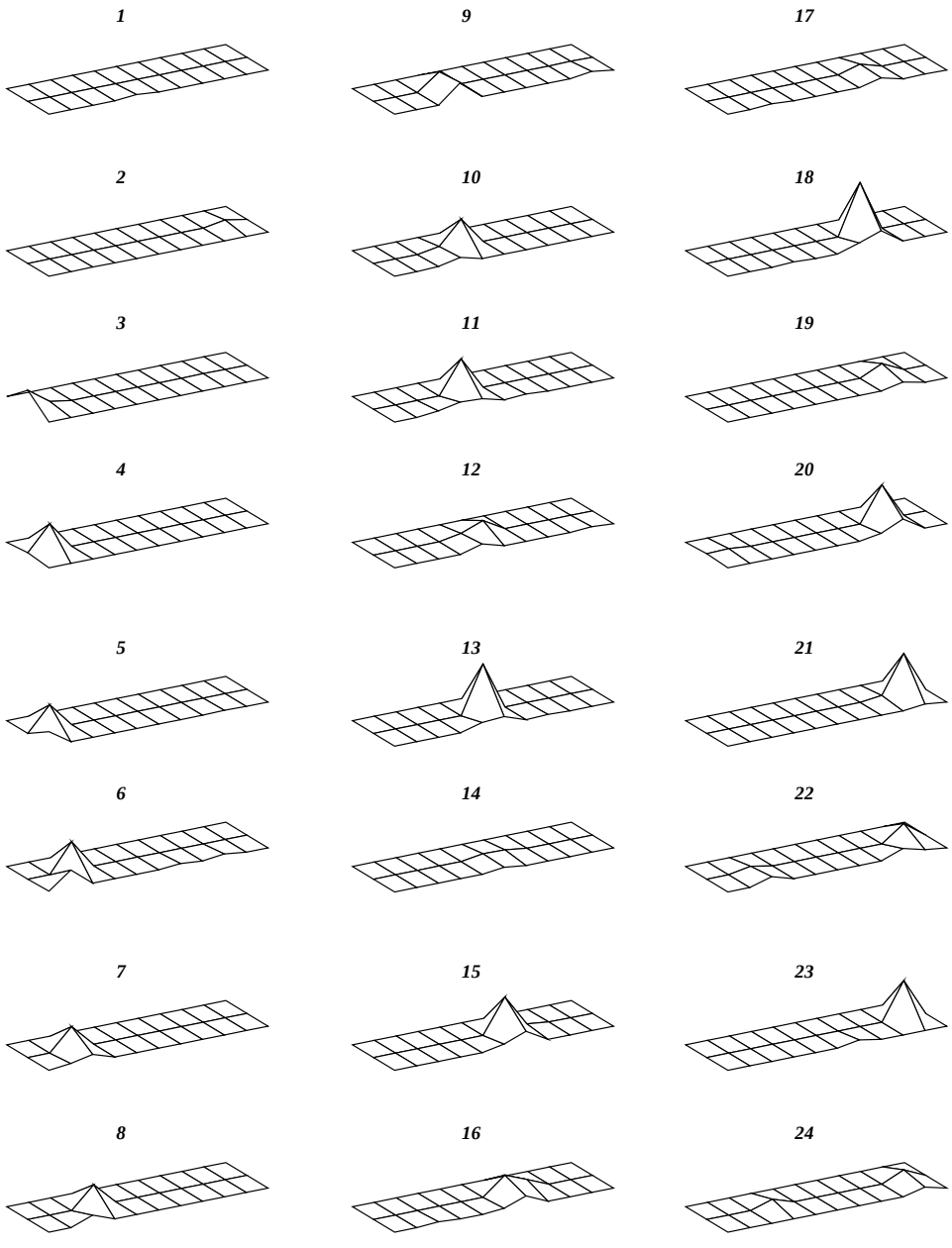

Figure 17. Same as in Figure 10 but for Test 7 of C-2.

unable to fit the data and to reproduce the moment rate distribution in space and time, when a different structure is used in the inverse model, in spite of good azimuthal coverage and many more stations (twelve) than is generally available for strong ground motion data. This is, however, the most realistic case and sug-

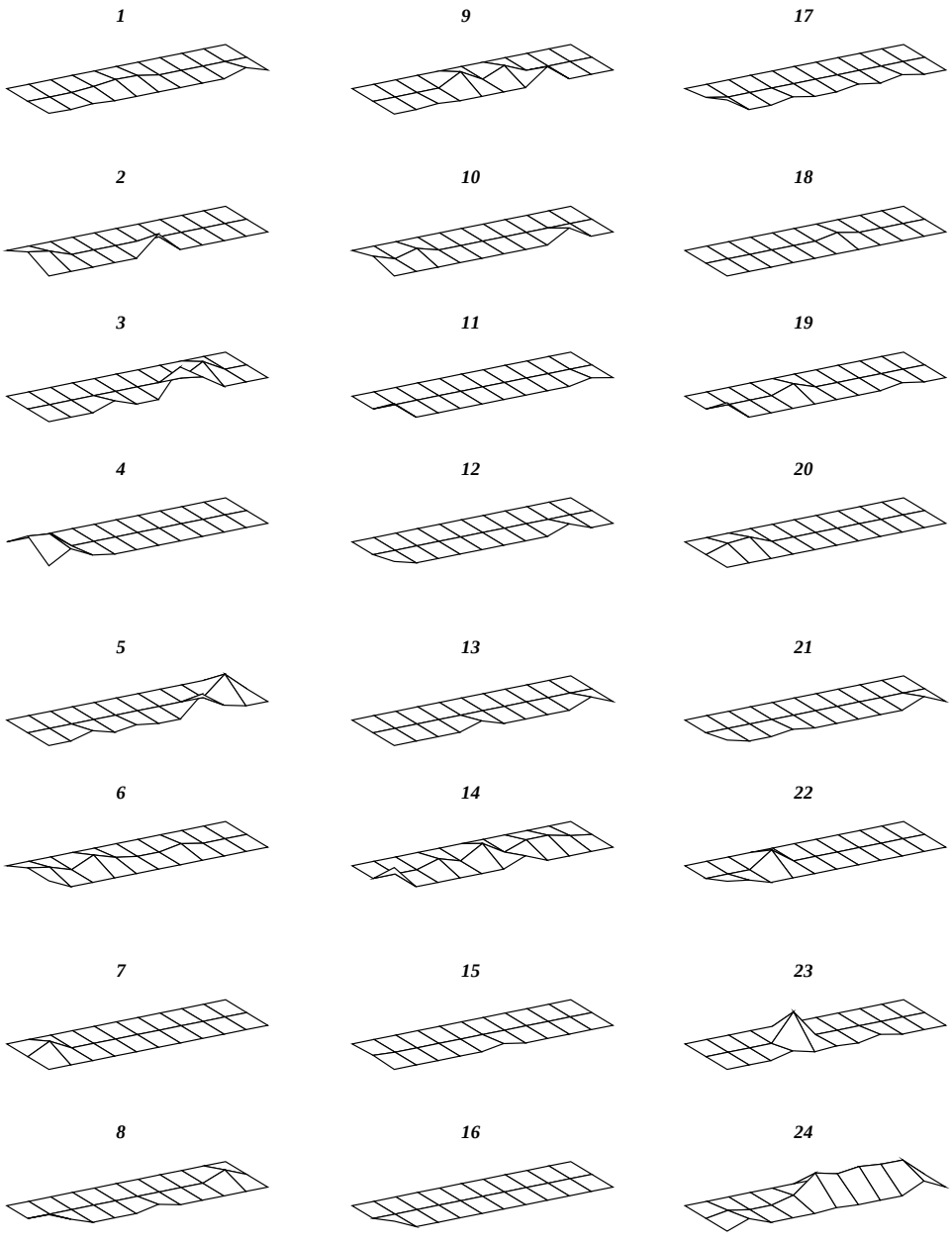

Figure 18. Same as in Figure 10 but for Test 7 of C-4.

gests that good structural information at the source is essential to reliably determine the seismic moment rate history and distribution on a fault.

Test 13 – We performed an inversion using the much shorter time window of 20s of data to see if the solution

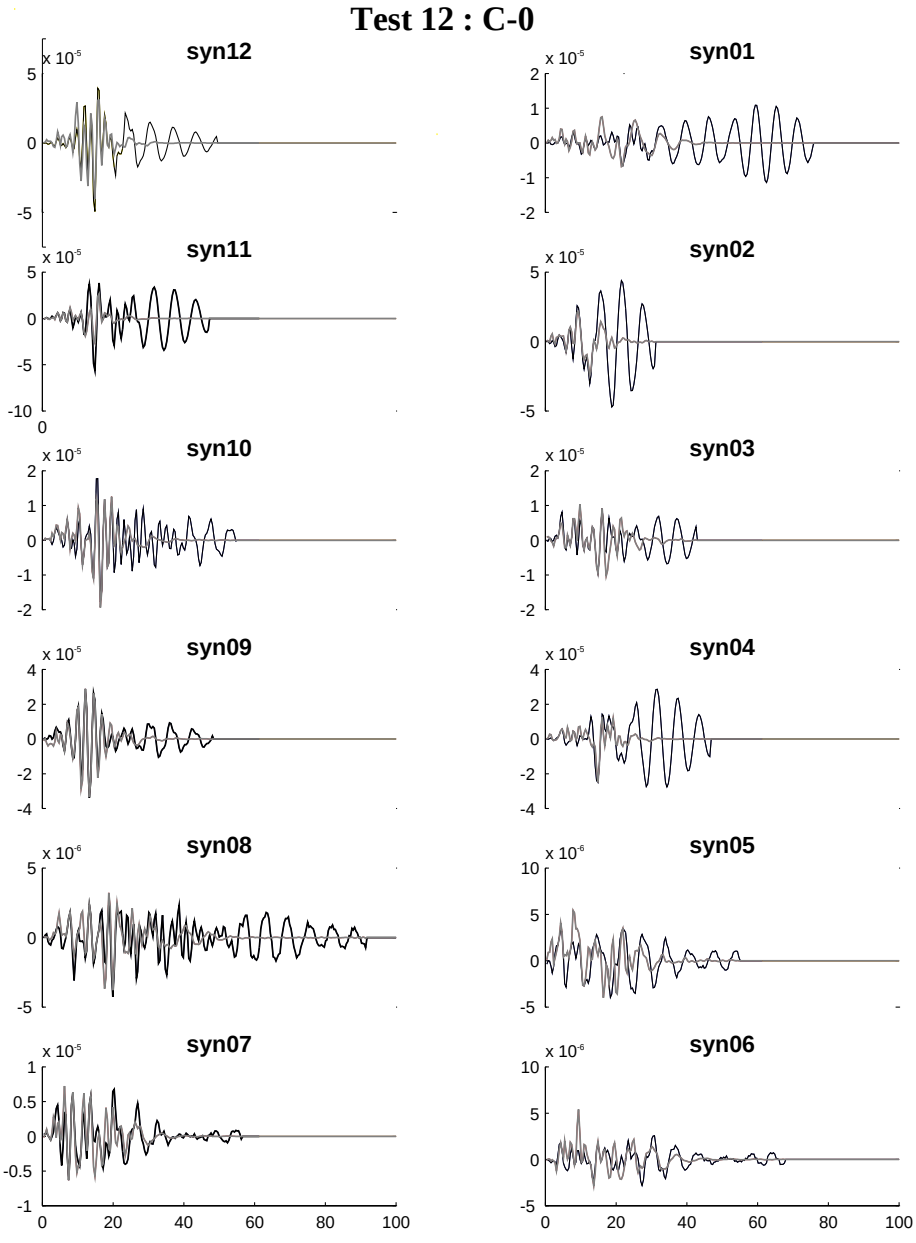

Figure 19. The comparison of the artificial data (solid lines) to the solution accelerograms (dotted lines) for Test 12 for C-0.

is affected. We find that the data are still not well fitted and the solution does not improve.

Results for the 20 km × 10 km fault

Till now, we have considered a fault with an aspect ratio of 1 to 5 which is mainly seen for great events (the 1957 Rat Island earthquake, the 1960 Chilean earthquake, the 1964 Alaska earthquakes, for example) but not usually for smaller events. So we study a fault with the aspect ratio of 1 to 2 which is close to the typical aspect ratio seen for shallow thrust faults (Wells & Coppersmith, 1994). We consider a fault that is 20 km long and 10 km wide. The top of the fault is at 5 km and the tests we performed are reported in the flow-

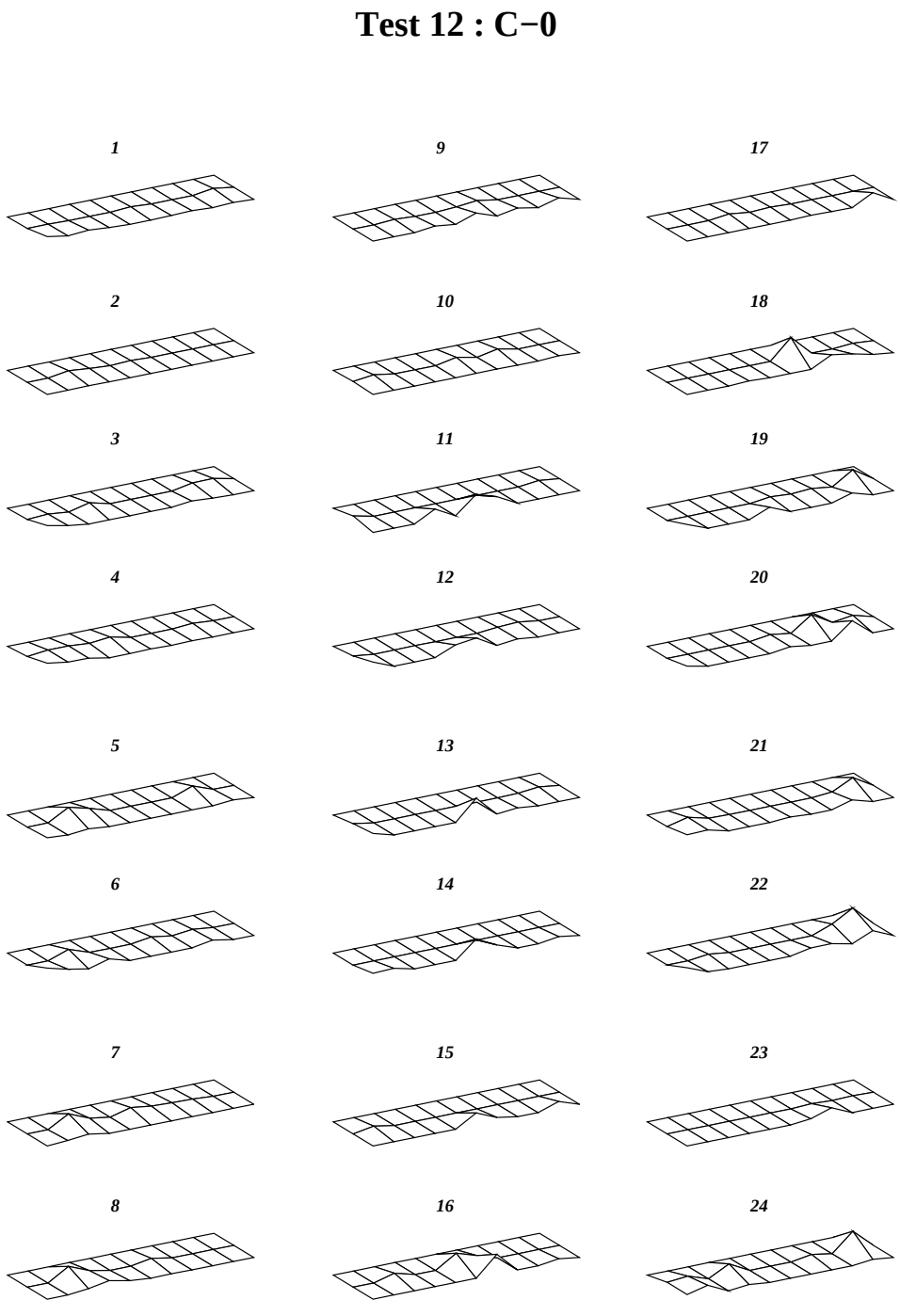

Figure 20. The moment rate maps in time produced by the inversion in Test 12 for C-0.

chart of Figure 5b and in Table 1. With the new fault geometry, we repeated most of the tests of the previous section for Cases 1 and 2 (Table 1); we inverted for the same grid size in space and in time for the forward and the inverse case, as well as for larger cells sizes in the inversion than in the forward case; we also added 5% of noise as we did before. Our main results do not change due to the changing of the aspect ratio, as it

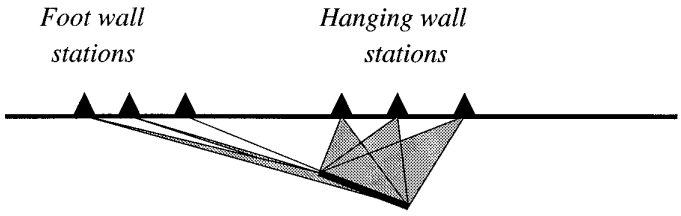

Figure 21. Schematic explanation of the difference between the illumination of the fault by stations located on the foot wall and on the hanging wall.

can be seen by the values of the misfit we report in Figure 16b.

Discussion and Conclusions

The aim of this study was to determine how reliably one can invert accelerograms to determine the rupture process details, when the station configuration is less than optimal. We show that the solutions can be improved by using well-established physical constraints, to reduce the effect of the less-than-optimal station coverage in the inversion. In some cases, we deliberately chose a very unfavorable scenario, since our purpose was to determine which properties of the faulting process could still be reliably obtained, if any.

For a dipping fault, we show that the best configuration is when the stations are on the hanging wall and six stations on the hanging wall are enough to obtain the moment rate history and distribution. The stations on the hanging wall are closer to the fault surface but the better result is also due to the better illumination of the fault by the hanging wall stations, as is illustrated schematically in Figure 21. Further, we find that the solution for the C-1 configuration, with six stations all located on the hanging wall side of the fault, is better than that for configuration C-0 with twelve uniformly distributed stations. It may appear surprising at first glance that adding the six footwall stations produces a poorer solution. But since the footwall stations illuminate the fault less well, their contribution to the Green function matrix A worsens its condition number. This provides incentive to install permanent ocean bottom strong ground motion stations in subduction zones. Thus the azimuthal distribution and the resulting illumination of the fault is more important than simply the number of stations. For a fault dipping more shallowly than that considered in this paper, the illumination effect discussed above will be even more pronounced.

Placing only four stations in the forward direction relative to the rupture propagation, was sufficient to recover the solution well. On the other hand, four stations placed in the backward direction produced a poorer solution, though the main features of the rupturing process were still obtained. Finally, we were unable to determine the details of the rupturing process when using a different source medium structure than the correct one, even though the overall picture of the moment rate distribution could still be recovered. Our point in using very different structure in the inversion was to show that though we can compensate for poor station coverage by using constraints, very incorrect structure cannot be compensated for by any means. Thus at regional distances using an incorrect source Earth structure, it is difficult to distinguish between the true source properties and artefacts generated by the incorrect medium properties, even with an optimal station distribution and additional physical constraints. Except in a very few intensively studied regions of the world (for example, California) the crustal structure unfortunately remains poorly known even today. Our study shows that some gross features of the faulting process can be obtained even in that case, though not the finer details.

Acknowledgements

We are very grateful to Dave Wald and an anonymous reviewer for a thorough review of the manuscript, which helped to improve it significantly. This study was partially supported by EC program, Environment and Climate, Topic IV.1.1, Natural Risks – Seismic Hazard, under the ENVIRONMENT contracts EN5V-CT94-0513 and ENV4-CT96-0296. The computations were done on the Cray J932-SN9522 at the Rutherford-Appleton Laboratories, Didcot, UK under a Supercomputing grant obtained through the Natural Environmental Research Council of the U.K. and on

the Cray J916/8-1024 at Centro di Calcolo of the University of Trieste, Italy.

References

Bernard, P., Gariel, J. C. & Dorbath, L., 1997. Fault location and rupture kinematics of the magnitude 6.8, 1992 Erzincan earthquake, Turkey from strong ground motion and regional records, *Bull. Seismol. Soc. Am.* **87**,5, 1230–1293.

Beroza, G. C. & Spudich, P., 1988. Linearized inversion for fault rupture behavior: application to the 1984, Morgan Hill, California earthquake, *J. Geophys. Res.* **93**, 6275–6296.

Das, S. & Kostrov, B. V., 1990. Inversion for seismic slip rate and distribution with stabilizing constraints: Application to the 1986 Andreanof Islands earthquake, *J. Geophys. Res.* **95**, 6899–6913.

Das, S. & Kostrov, B. V., 1994. Diversity of solutions of the problem of earthquake faulting inversion. Application to SH waves for the great 1989 Macquarie Ridge earthquake, *Phys. Earth Planet. Int.* **85**, 293–318.

Das, S. & Suhadolc, P., 1996. On the inverse problem for earthquake rupture. The Haskell-type source model, *J. Geophys. Res.* **101**, 5725–5738.

Das, S., Suhadolc, P. & Kostrov, B. V., 1996. Realistic inversions to obtain gross properties of the earthquake faulting process, *Tectonophysics*. In: C. Trifu (ed.), Special issue entitled Seismic Source Parameters: from Microearthquakes to Large Events **261**, 165–177.

Hartzell, S. H. & Heaton, T. H., 1983. Inversion of strong-ground motion and teleseismic waveform data for the fault rupture history of the 1979 Imperial Valley, California earthquake, *Bull. Seismol. Soc. Am.* **73**, 1553–1583.

Hwang, P. Y., 1985. Focal depths and mechanisms of mid-ocean ridge earthquakes from body waveform analysis, Ph. D. thesis, Massachusetts Institute of Technology, pp. 36–39.

Iida, M., Miyatake, T. & Shimazaki, K., 1990. Relationship between strong-motion array parameters and the accuracy of source inversion and physical waves, *Bull. Seismol. Soc. Am.* **80**, 1533–1552.

Iida, M., 1993. Source effects on strong-motion records and resolving power of strong-motion arrays for source inversion, *Tectonophysics* **218**, 179–193.

Kostrov, B. V. & S. Das, 1988. Principles of earthquake source mechanics, *Appl. Math. Mech. Ser.*, Cambridge University Press, New York, 286 pp.

Madariaga, R., 1977. High-frequency radiation from crack (stress drop) models of earthquake faulting, *Geophys. J.* **51**, 625–651.

Menke, W., 1985. Imaging fault slip using teleseismic waveforms: analysis of a typical incomplete tomography problem, *Geophys. J. Roy. As. Soc.* **81**, 197–204.

Miyatake, T., Iida, M. & Shiamazaki, K., 1986. The effects of strong motion array configuration on source inversion, *Bull. Seismol. Soc. Am.* **76**, 1173–1185.

Olson, A. H. & Anderson, J. G., 1988. Implications of frequency-domain inversion of earthquake ground motions for resolving the space-time dependence of slip on an extended fault, *Geophys. J.* **94**, 443–455.

Panza, G. F. & Suhadolc, P., 1987. Complete strong motion synthetics. In: B. A. Bolt (ed.) Seismic Strong Motion Synthetics, Computational Tecniques 4, Academic Press, Orlando, pp. 153–204.

Satake K., 1985. Effects of station coverage on moment tensor inversion, *Bull. Seismol. Soc. Am.* **75**, 1657–1667.

Stump, B. W. & Johnson, L. R., 1977. The determination of source properties by the linear inversion of seismograms, *Bull. Seismol. Soc. Am.* **67**, 1489–1502.

Wells, D. L. & Coppersmith, K. J., 1994. New empirical relationships among magnitude, rupture length, rupture width, rupture area, and surface displacement, *Bull. Seismol. Soc. Am.* **84**, 974–1002.